Supplementary Information

Enhancing CO_2 hydrogenation to methanol via synergistic effect of MoS_2 interlayer spacing and sulfur vacancy

Langlang Qin[a], Yunfei Gao[*b], Caiyun Han[a], Minghui Zhu[d], Shuang Wang[*a,c]

[a.] College of Environmental Science and Engineering, Taiyuan University of Technology, Jinzhong 030600, Shanxi, P.R. China.

[b.] Institute of Clean Coal Technology, East China University of Science and Technology, Shanghai 200237, P.R. China.

[c.] Shanxi Key Laboratory of Gas Energy Efficient and Clean Utilization, Taiyuan University of Technology, Taiyuan 030024, Shanxi, P.R. China.

[d.] State Key Laboratory of Chemical Engineering, School of Chemical Engineering, East China University of Science and Technology, Shanghai 200237, PR China

E-mail: yunfeigao@ecust.edu.cn
wangshuang@tyut.edu.cn

Materials

Sodium molybdenum oxide anhydrous (Na_2MoO_4) was purchased from Aladdin. Thioacetamide (C_2H_5NS), Hydrazine hydrate aqueous solution (N_2H_4 H_2O), Ammonia liquor (25%, $NH_3{\cdot}H_2O$) and Sodium borohydride ($NaBH_4$) were purchased from Sinopharm reagent Group Co., Ltd.

Methods

Synthesis of MoS_2-NH_3: In a typical synthetic procedure, X mL (X = 25, 35.7, and 50) $NH_3{\cdot}H_2O$ were added to 300 mg of the MoS_2 samples and reacted for 3 h to obtain different S-vacancy concentrations. The resultant black precipitate was collected using centrifugation at 5000 rpm/min. Then, the collected material was vacuum-dried overnight at 70 °C, named MoS_2-NH_3.

Synthesis of MoS_2-$NaBH_4$: Briefly, 300 mg of MoS_2 samples and X mg (X = 38, 76, and 760) of $NaBH_4$ were dissolved in 50 mL of deionized water to form a homogeneous transparent solution and reacted for 3 h to obtain different S-vacancy concentrations. The resultant black precipitate was collected using centrifugation at 5000 rpm/min. Then, the collected material was vacuum-dried overnight at 70 °C, named MoS_2-$NaBH_4$.

DFT calculations:

DFT calculations were performed using the Vienna Ab initio Simulation Package (VASP).[1, 2] The electron interaction energy of exchange correlation was described by using generalized gradient approximation (GGA) with the function of Perdew–Burke–Ernzerhof (PBE). The valence electrons were treated with a plane-wave basis sets with a cutoff kinetic energy of 400 eV. The Brillouin zone integration was sampled at the Γ-point for energy calculations and 2 × 2 × 1 Monkhorst−Pack mesh k-points for electronic structure analysis. The convergence criterion of force and energy were set as

0.03 eV/Å and 1×10^{-3} eV for all structural optimizations, respectively. The DFT-D3 correction method was employed to consider van der Waals interactions.[3] The monolayer model of MoS_2 (5 × 5) was used to construct the substrate with lattice parameters of a = b = 16.00 Å. To prevent interactions between periodic structures, a 15 Å vacuum space was incorporated along the z-direction. All atoms were allowed to relax during the structural optimization process.

Material characterizations:

The X-ray diffraction (XRD) patterns were obtained with X-ray diffractometer (Panalytical Aeris, Holland) operating at Cu Kα radiation (λ = 1.5418 Å). The X-ray photoelectron spectroscopy (XPS) measurements were performed by using an ESCALAB 250Xi electron spectrometer (Thermo Scientific Corporation) with monochromatic 150 W Al Kα radiation. The morphology and structure of the samples were investigated by field-emission scanning electron microscopy (FESEM; SU8010, Japan). Transmission electron microscopy (TEM) with energy dispersive X-ray spectroscopy (EDS) and high-resolution TEM (HRTEM) results were obtained using a JEM-2100F electron microscope with an accelerating voltage of 200 kV. Raman spectra were obtained on a Renishaw InVia Raman spectrometer with the 514 nm excitation line of an Ar ion laser.

Temperature-programmed CO_2 desorption (CO_2-TPD): CO_2-TPD were carried out using a Micromeritics AutoChem II 2920 chemisorption instrument. During the CO_2-TPD, approximately 50 mg of sample was first pretreated under He flow (30 mL·min^{-1}) at 150 °C for 1 h. The sample was subsequently heated to 300 °C and purged for 3 h with 10% H_2/Ar mixture at a flow rate of 30 mL min^{-1} to fully reduce the catalysts and then cooled to 50 °C. The sample was purged with 10% CO_2/He mixture (30 mL·min^{-1}) for 1.5 h at 50 °C to saturate the surface, then purged in flowing He (30 mL·min^{-1}) for

1 h to remove physically adsorbed CO_2. Subsequently, the temperature was elevated in flowing He (30 mL·min^{-1}) until up to 900 ºC at a ramp rate of 10 ºC·min^{-1}. CO_2 desorption amount was quantitatively measured based on CO_2 single-pulse experiment.

Brunauer–Emmett–Teller surface area measurements were performed on a V-Sprb 4804TP Surface Area Analyzer. Prior to N_2 adsorption, the samples were degassed under vacuum at 120 °C for 6h.

Catalytic tests:

The catalyst performance was evaluated on a continuous fixed reaction bed. First of all, 0.3 g catalyst were loaded into a stainless steel reaction tube, and filled with quartz sand of equal size up and down. Typically, before the reaction, catalyst was pretreated in situ with 30 mL min^{-1} H_2 at 1 bar and 300 °C for 3 h. After the reduction, the reactant was introduced into the reactor. The reactions were performed under a pressure of 30 or 50 bar and in a temperature range from 180 to 260 °C, with a H_2/CO_2 ratio of 3:1 and GHSVs from 8000 to 16000 ml $g_{cat.}^{-1}$ h^{-1}. The products were analyzed using an online gas chromatograph equipped with a thermal conductivity detector (TCD) and a flame ionization detector (FID). A TDX-01 packed column was connected to the TCD and an RT-Q-BOND-PLOT capillary column was connected to the FID. Product selectivity was calculated on a molar carbon basis. The catalytic performances during the stable phase of the reaction were typically used for discussion.

The reaction parameters including CO_2 conversion, product selectivity, and methanol space-time yield (STY_{CH_3OH}) were calculated as follows

$$CO_2\ conversion\ \% = \frac{n_{CO_2,in} - n_{CO_2,\,out}}{n_{CO_2,in}} \times 100$$

$$product\ selectivity\ \% = \frac{n_{product}}{\sum n_{product}} \times 100$$

$$STY_{CH3OH}\left(g \cdot g_{cat}{}^{-1} \cdot h^{-1}\right) = n_{CH3OH} \times \frac{M_{CH3OH}}{m_{MoS_2}} \times 60\left(min\ h^{-1}\right) \times 0.001\left(mol\ mmol^{-1}\right)$$

where $n_{CO_2,\ in}$ and $n_{CO_2,\ out}$ are the amounts of CO_2 (mol) at the inlet and outlet of the reactor and $n_{product}$ is the amount of product (mol) at the outlet of the reactor. m_{MoS_2} is the weight of MoS_2 in the catalyst (g), and M_{CH_3OH} is the molecular weight of methanol (32.04 $g \cdot mol^{-1}$).

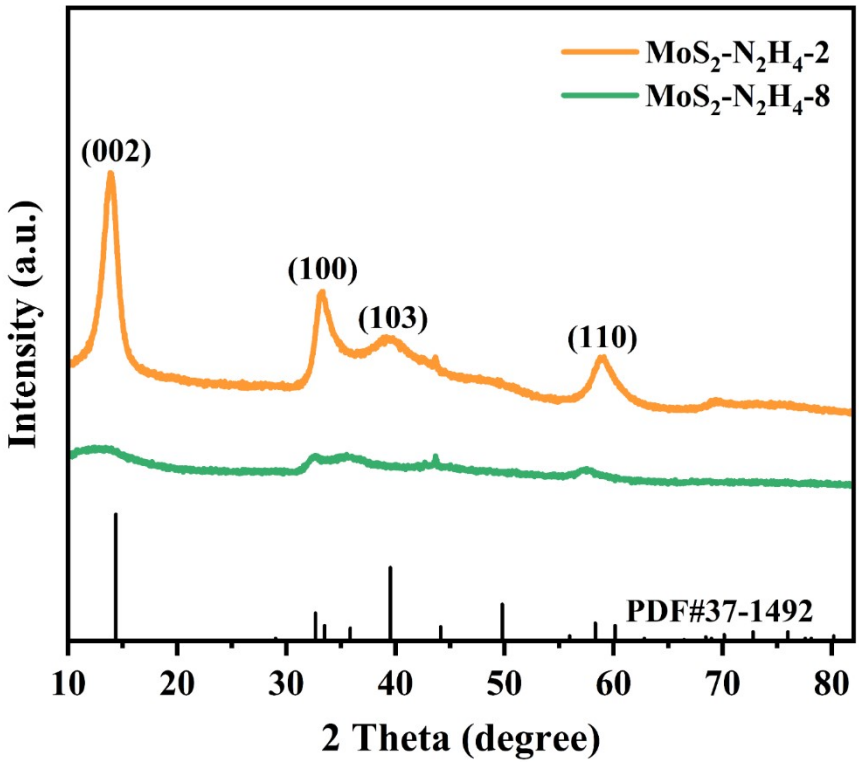

Fig. S1. XRD patterns of MoS_2-N_2H_4-8, MoS_2-NH_3 and MoS_2-$NaBH_4$ catalysts.

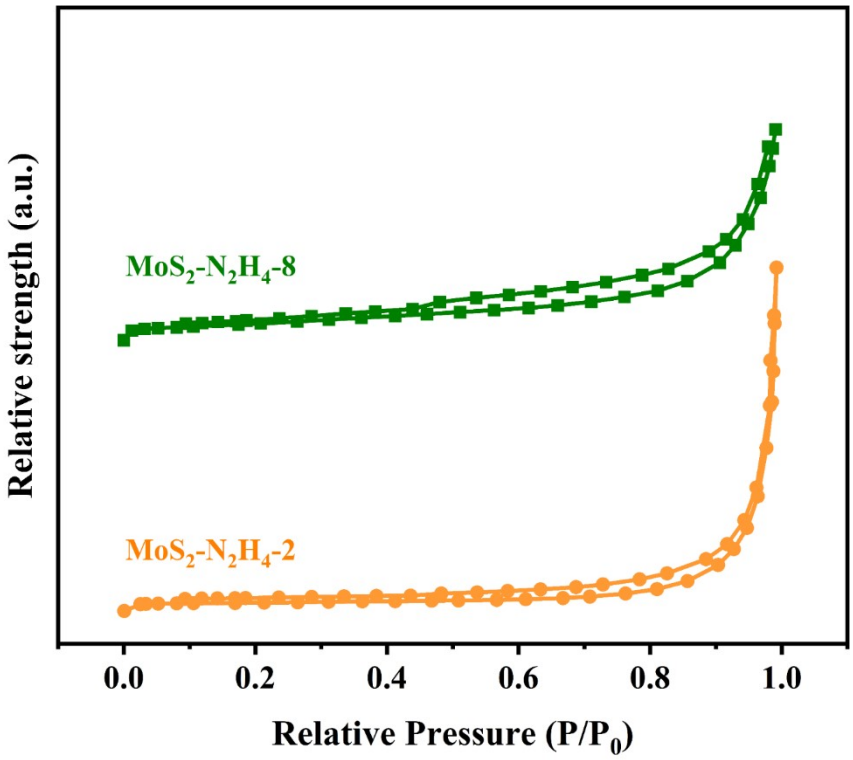

Fig.S2. N_2 adsorption-desorption isotherms of MoS_2-N_2H_4-2, MoS_2-N_2H_4-8 catalysts.

Table S1

Specific surface area and particle size of MoS_2, MoS_2-N_2H_4-2, MoS_2-N_2H_4-4, MoS_2-N_2H_4-8, MoS_2-NH_3 and MoS_2-$NaBH_4$ catalysts.

Catalysts	Specific surface area (m^2/g)	Particle size (nm)[a]	d(002) (nm)[b]
MoS_2	16.078	3.75	0.642
MoS_2-N_2H_4-2	21.889	1.79	0.713
MoS_2-N_2H_4-4	26.1175	0.86	0.728
MoS_2-N_2H_4-8	30.054	2.14	0.730
MoS_2-NH_3	37.4748	3.43	0.734
MoS_2-$NaBH_4$	26.545	1.04	0.635

[a] calculated by Scherrer equation using XRD data.

[b] calculated by Bragg's Law using XRD data.

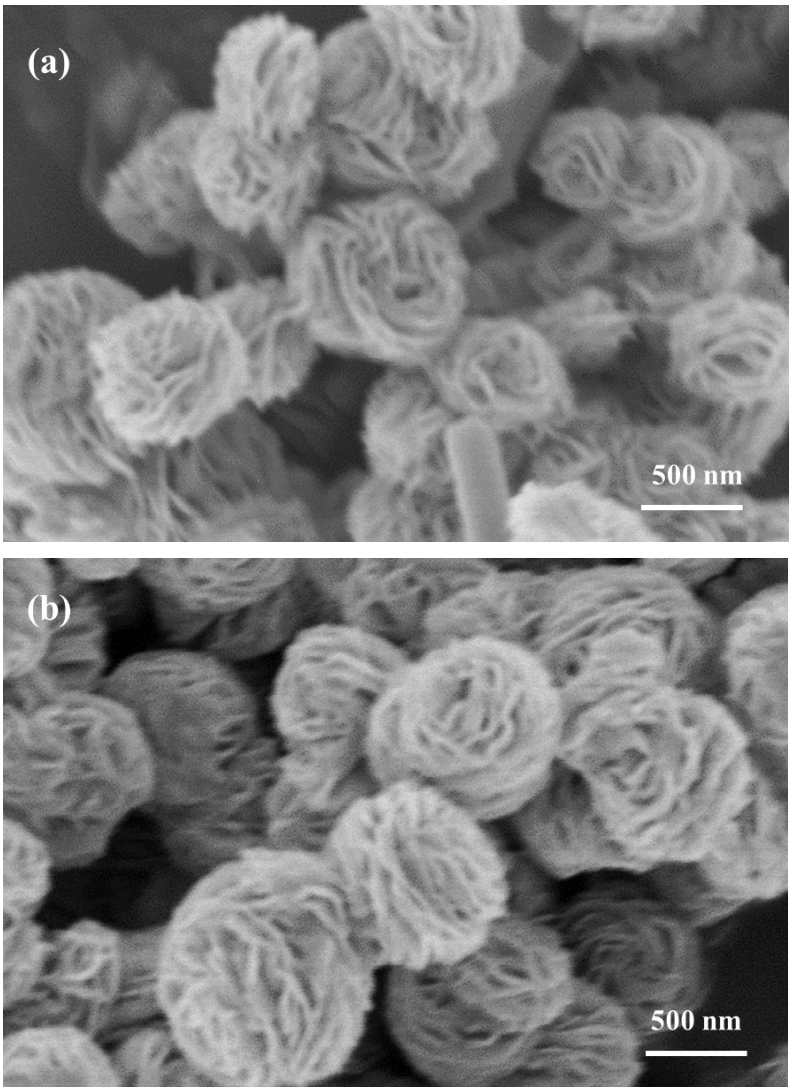

Fig. S3. SEM images of (a) MoS_2-N_2H_4-2 and (b) MoS_2-N_2H_4-8 catalysts.

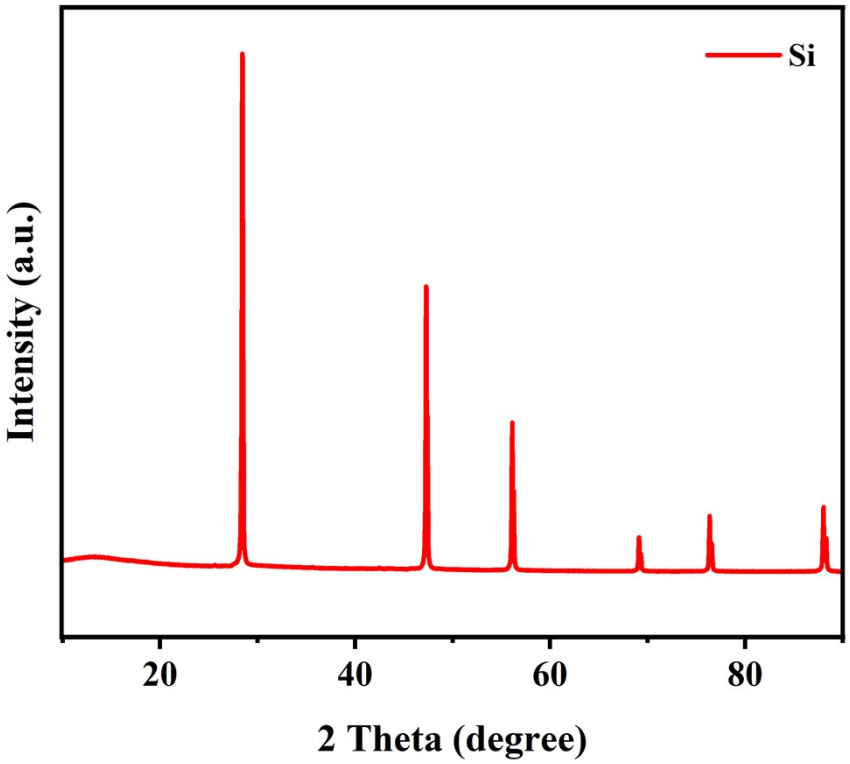

Fig. S4. XRD patterns of Si standard sample.

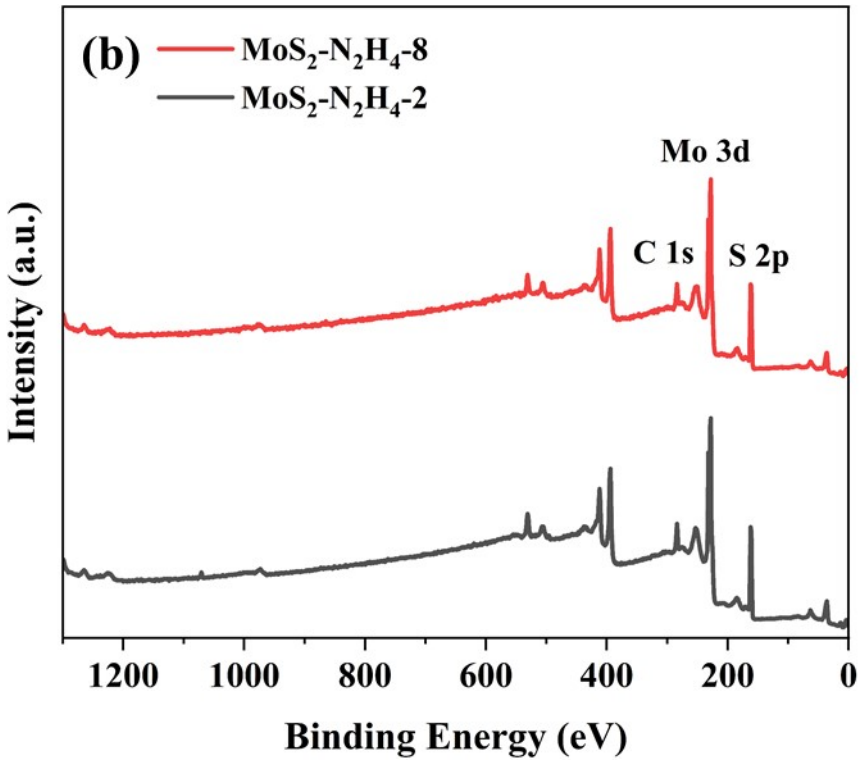

Fig. S5. The XPS survey spectra of MoS_2-N_2H_4-2, MoS_2-N_2H_4-8 catalysts.

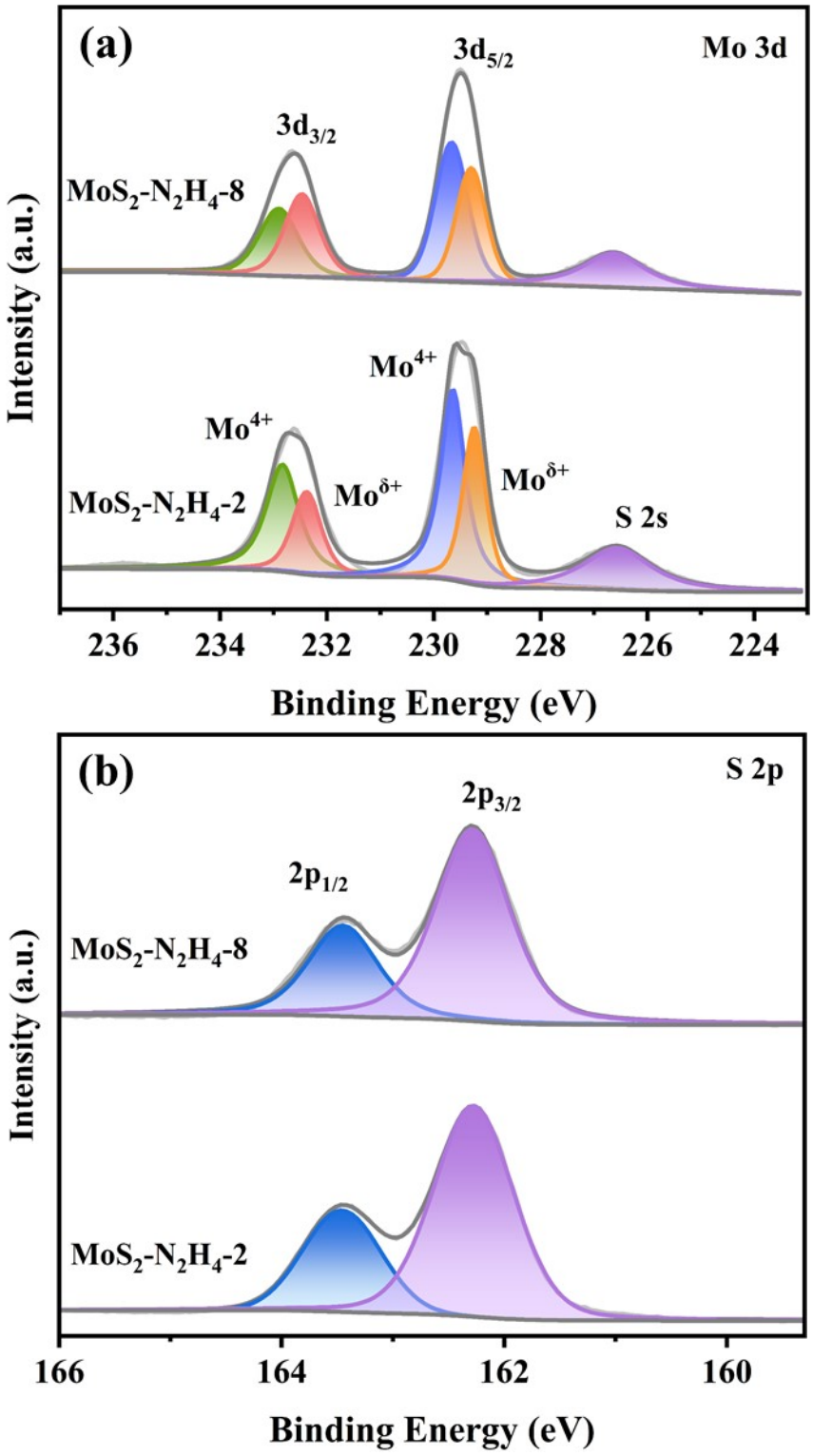

Fig. S6. XPS spectra of (a) Mo 3d and (b) S 2p states in MoS_2-N_2H_4-2 and MoS_2-N_2H_4-8 catalysts.

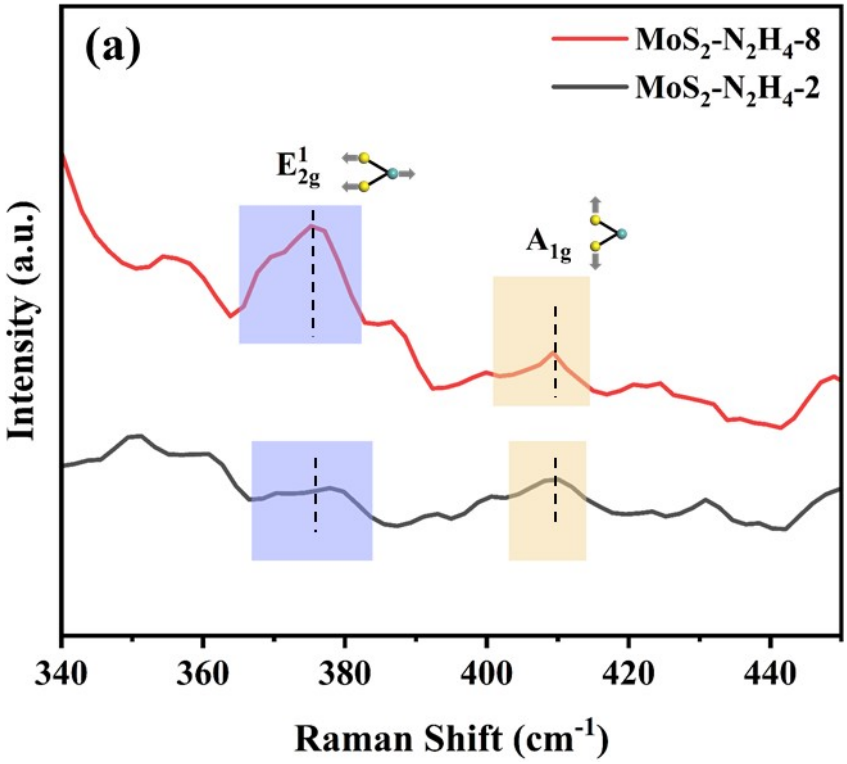

Fig. S7. Raman spectra of MoS_2-N_2H_4-2 and MoS_2-N_2H_4-8 catalysts.

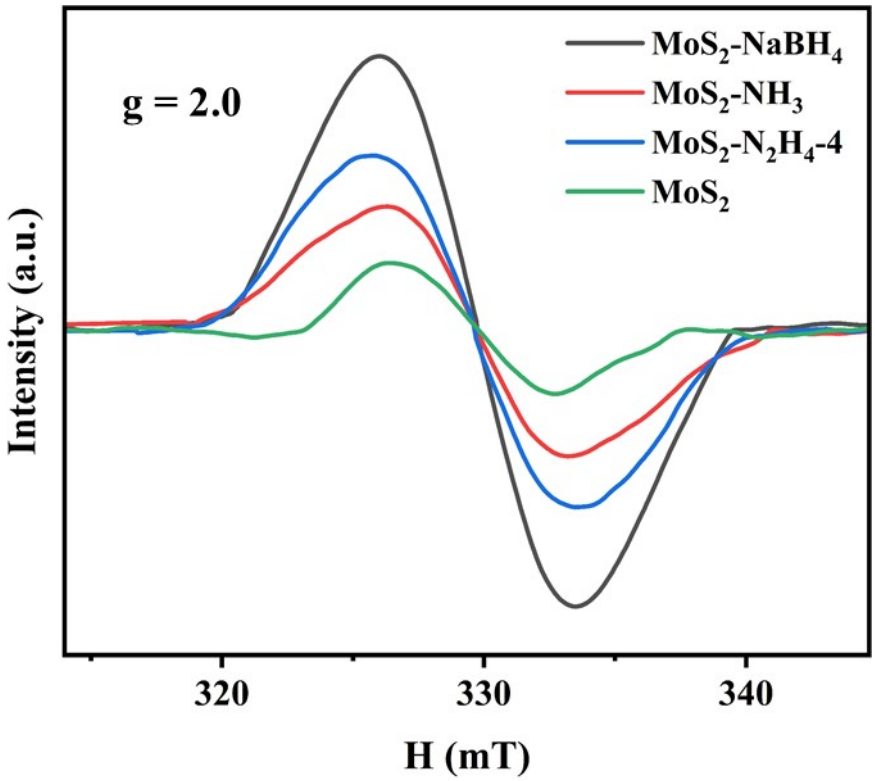

Fig. S8. The EPR spectra of MoS_2, MoS_2-N_2H_4-4, MoS_2-NH_3 and MoS_2-$NaBH_4$ catalysts.

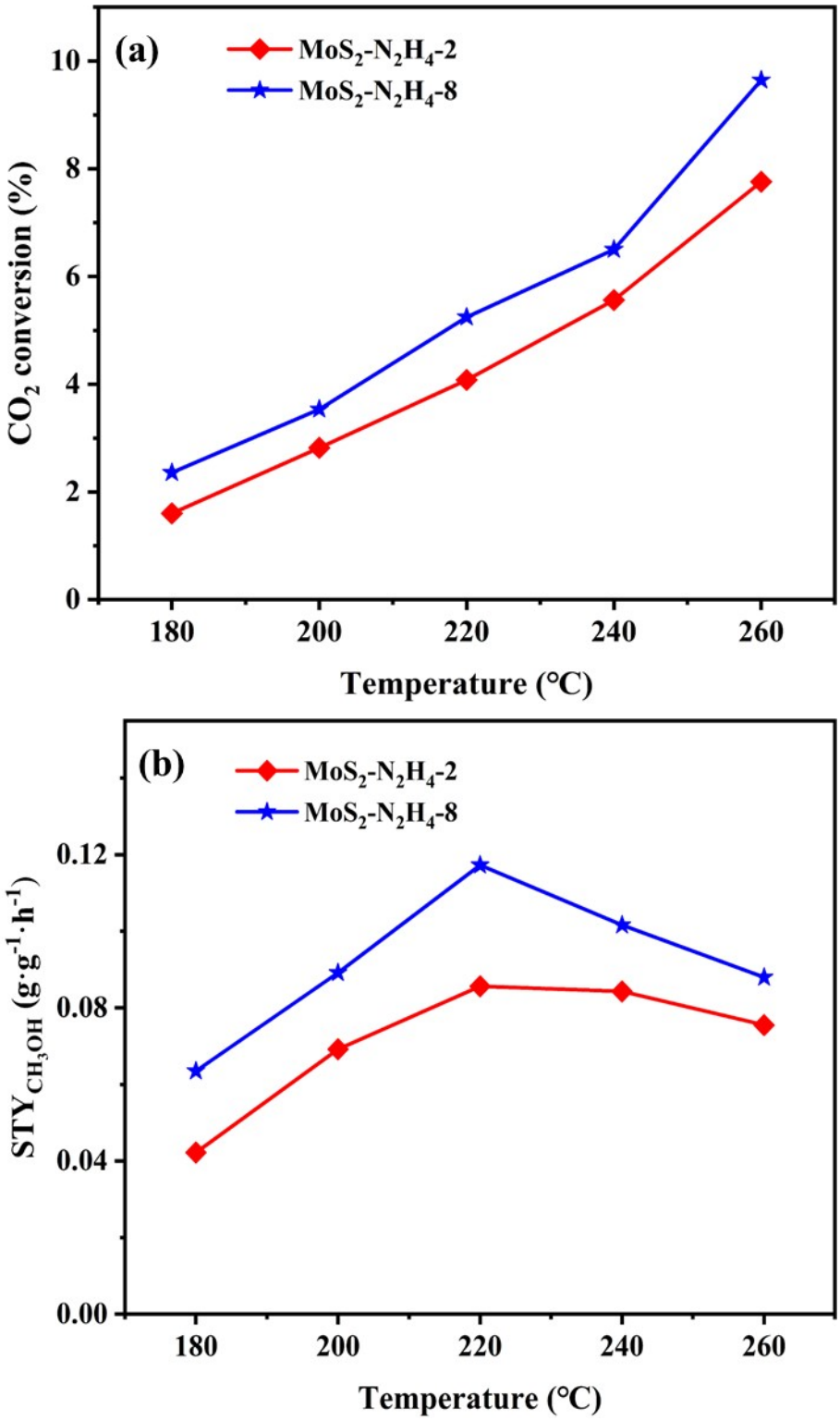

Fig. S9. (a) CO_2 conversion and (b) STY of CH_3OH over MoS_2-N_2H_4-2 and MoS_2-N_2H_4-8 catalysts. Reaction conditions: V_{CO_2/H_2} = 3/1, GHSV = 8000 mL·g_{cat}^{-1}·h^{-1}, P = 4.0 MPa.

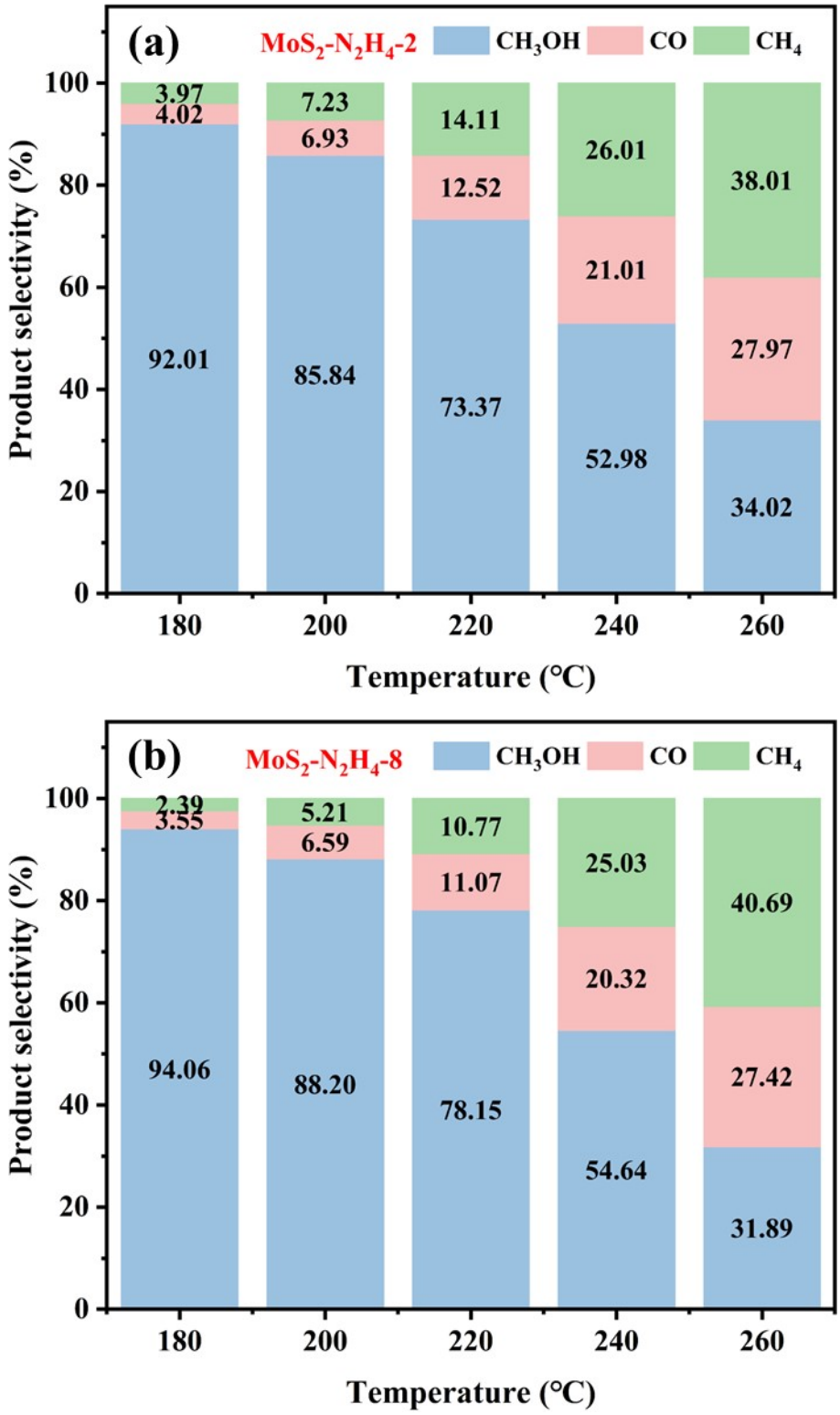

Fig. S10. Product selectivity over (a) MoS_2-N_2H_4-2 catalyst and (b) MoS_2-N_2H_4-8 catalyst. Reaction conditions: V_{CO_2/H_2} = 3/1, GHSV = 8000 mL·g_{cat}^{-1}·h^{-1}, P = 4.0 MPa.

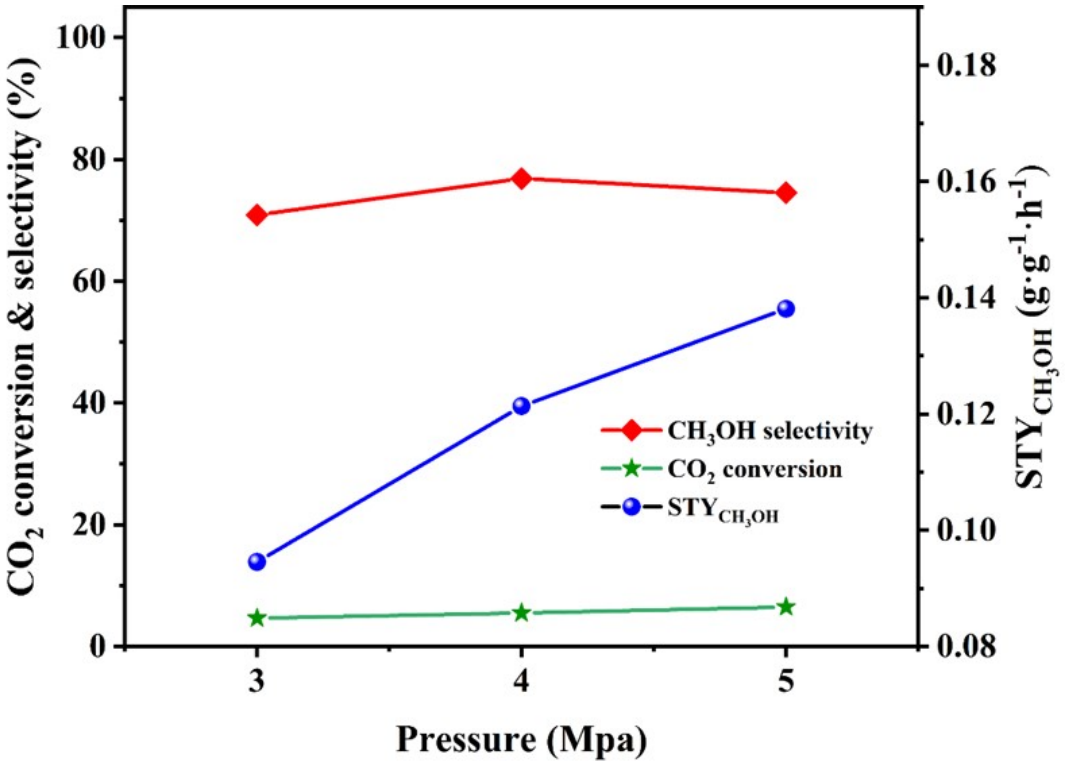

Fig. S11. Effect of pressure on CO_2 hydrogenation over MoS_2-N_2H_4-4 catalyst. Reaction conditions: 220 °C, V_{CO_2/H_2} = 1:3, GHSV = 8000 mL·g_{cat}^{-1}·h^{-1}.

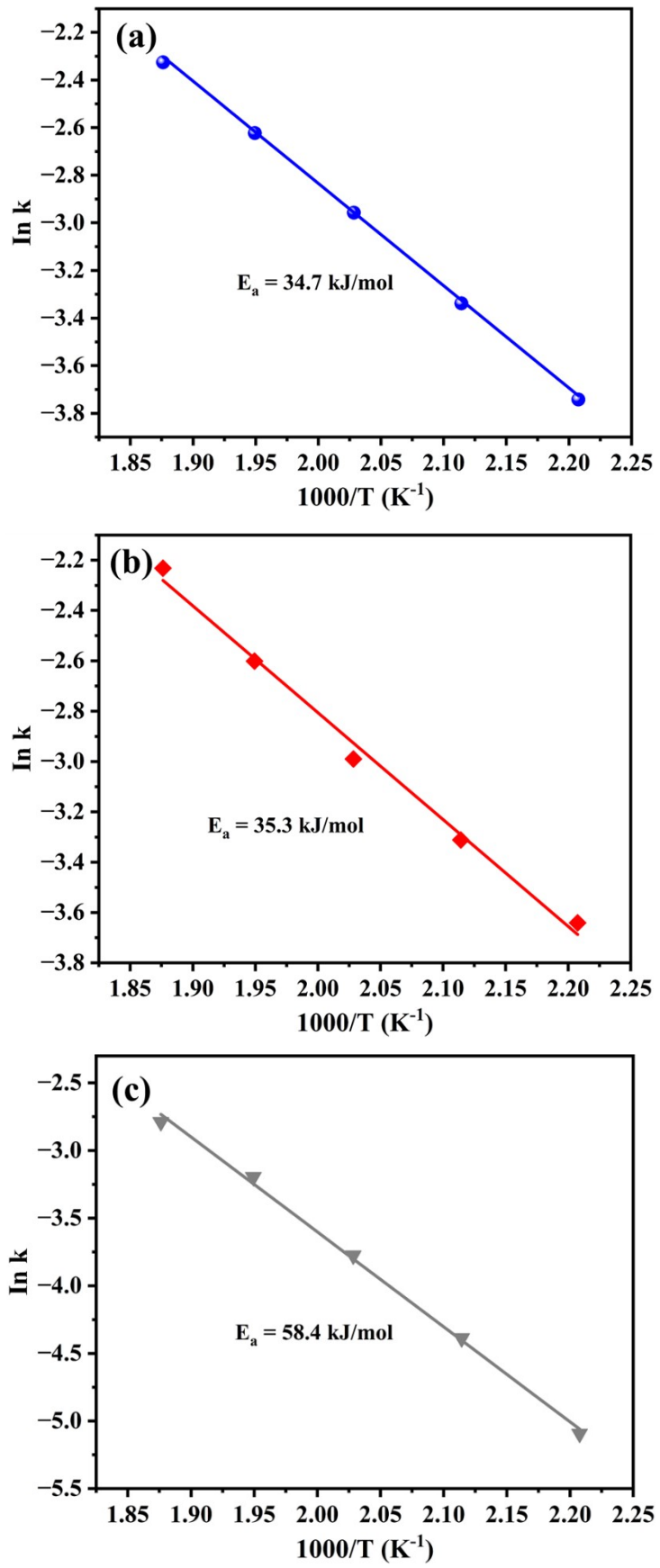

Fig. S12. Arrhenius plots and apparent activation energy of (a) MoS_2-N_2H_4-4, (b) MoS_2-NH_3 and (c) MoS_2-$NaBH_4$ catalysts.

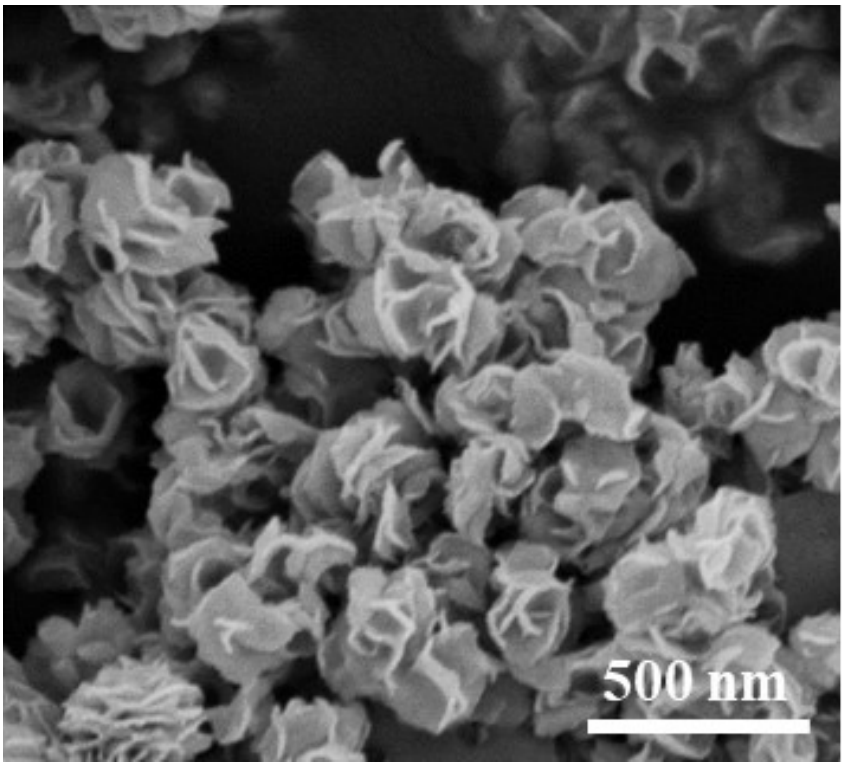

Fig. S13. SEM image of MoS_2-N_2H_4-4 catalyst after reaction.

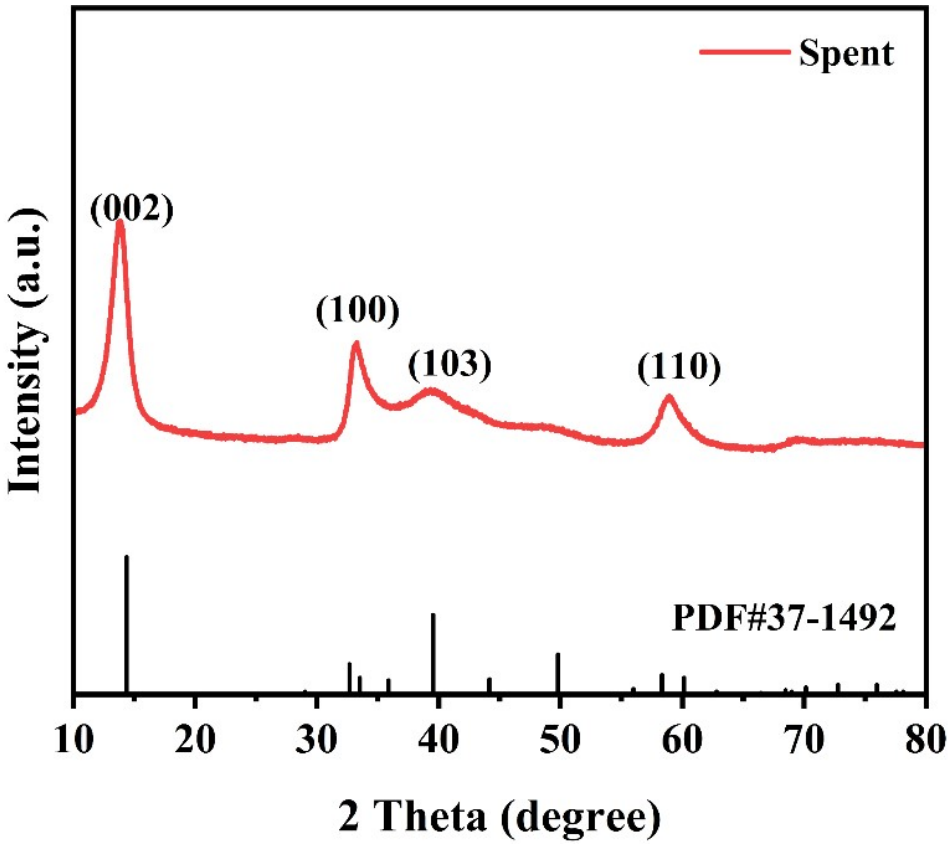

Fig. S14. XRD patterns of MoS_2-N_2H_4-4 catalyst after reaction.

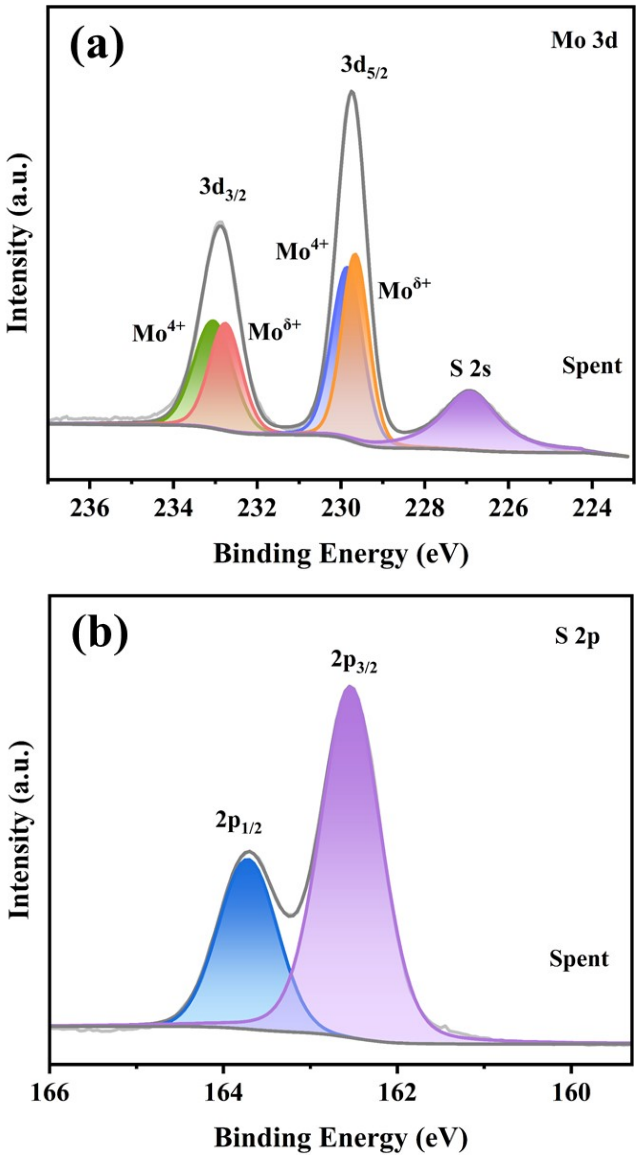

Fig. S15. XPS spectra of (a) Mo 3d and (b) S 2p states in MoS_2-N_2H_4-4 catalyst after reaction.

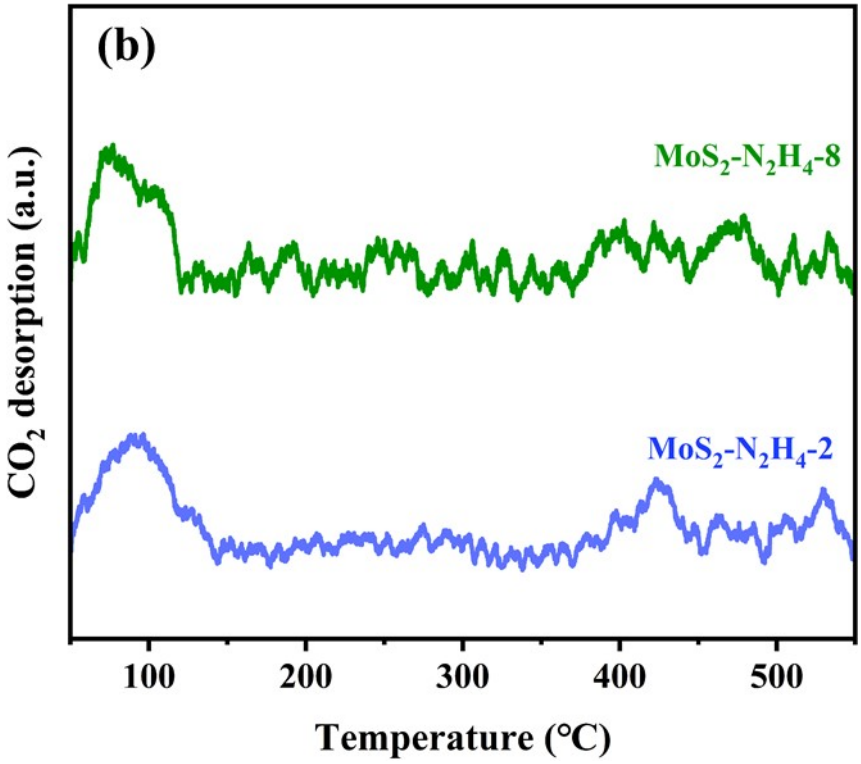

Fig. S16. CO_2-TPD profiles of MoS_2-N_2H_4-2 and MoS_2-N_2H_4-8 catalysts.

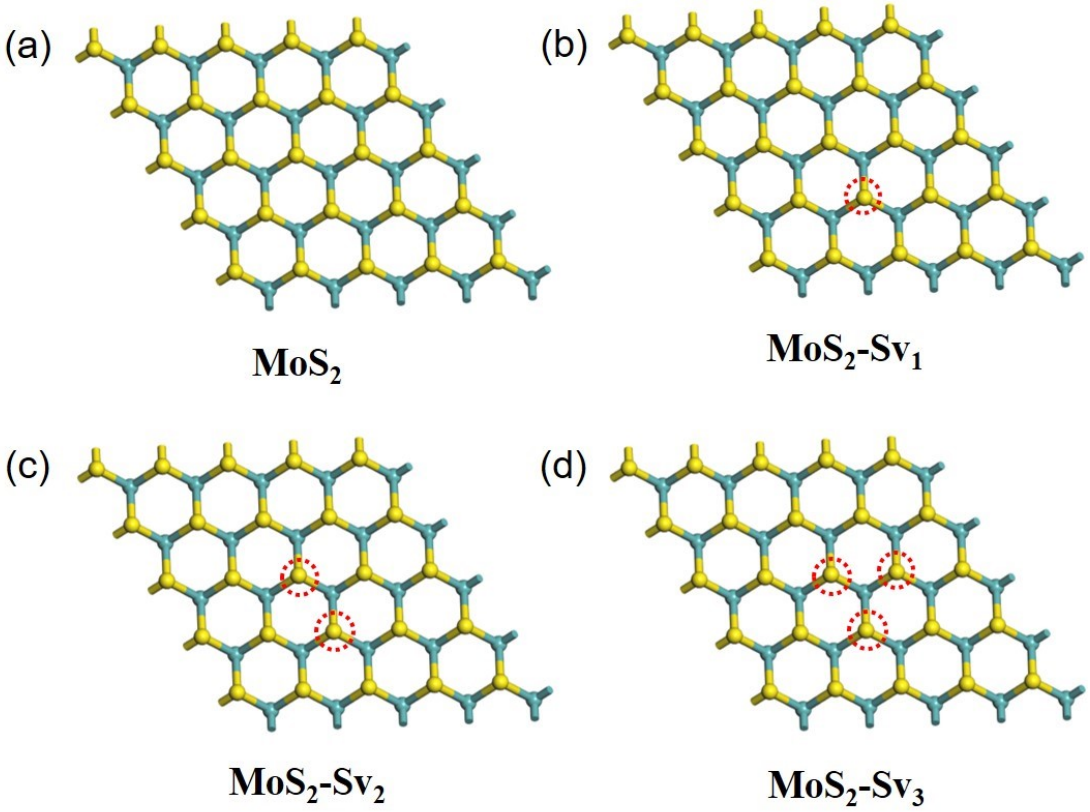

Fig. S17. DFT model of (a) MoS_2, (b) MoS_2-Sv_1 (c) MoS_2-Sv_2 and (d) MoS_2-Sv_3 catalysts.

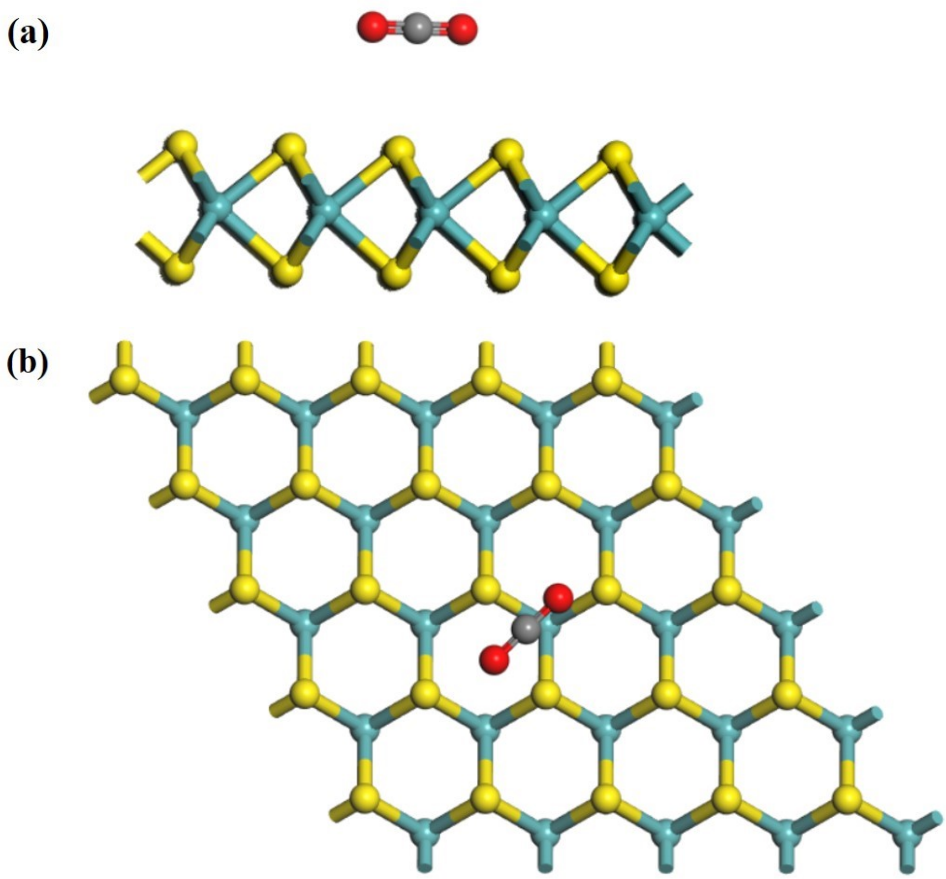

Fig. S18. Structural model diagram, (a) the side view and (b) the top view of CO_2 adsorption on MoS_2. Color sign: S in yellow, Mo in cyan, O in red, C in black.

Table S2 The catalytic performances of MoS_2-N_2H_4-4 catalyst and the reported partial catalysts for CO_2 hydrogenation to methanol.

Catalysts	*T* (°C)	P (Mpa)	GHSV ($mL \cdot g_{cat.}^{-1} h^{-1}$)	CO_2 Conv. (%)	CH_3OH Sel. (%)	STY_{MeOH} ($g_{MeOH} \cdot g_{cat}^{-1} \cdot h^{-1}$)	STY_{MeOH} ($g_{MeOH} \cdot g_{MoS_2}^{-1} \cdot h^{-1}$)	Ref.
MoS_2-N_2H_4	220	4	8000	5.52	76.8	0.1214		This
MoS_2-N_2H_4	220	5	8000	6.48	75.5	0.14		work
FL-MoS_2	180	5	3000	12.5	94.3	0.132		
FL-MoS_2	240	5	15000	11.0	81.4	0.49		[4]
ML-MoS_2	180	5	3000	8	80.7	0.074		
TL-MoS_2	180	5	3000	1.6	87.9	0.016		
h-MoS_2	240	5	6000	16	50	0.28		[5]
h-MoS_2/ZnS	260	5	6000	15.8	65.1	0.17		
MoS_2/Ni0.2	260	5	12000	1	83.76	-		[6]
MoS_2/Co0.2	260	5	12000	0.5	73.82	-		
5%Cu-MoS_2	220	4	12000	3	80		0.15	[7]
5%Cu-MoS_2	220	5	12000	5.39	85.95		0.25	
MoS_2@SiO_2	260	5	8000	11.1	52.2		0.165	[8]

References:

1. S. Zhou, W. Ma, U. Anjum, M. Kosari, S. Xi, S. M. Kozlov and H. C. Zeng, Nat. Commun., 2023, **14**, 5872.

2. X. Ma, L. Diao, Y. Wang, L. zhang, Y. Lu, D. Li, D. Yang and X. She, Chem. Eng. J., 2023, **457**, 141116.

3. G. Kresse and J. Hafner, Phys. Rev. B, 1994, **49**, 14251-14269.

4. J. T. Hu, L. Yu, J. Deng, Y. Wang, K. Cheng, C. Ma, Q. H. Zhang, W. Wen, S. S. Yu, Y. Pan, J. Z. Yang, H. Ma, F. Qi, Y. K. Wang, Y. P. Zheng, M. S. Chen, R. Huang, S. H. Zhang, Z. C. Zhao, J. Mao, X. Y. Meng, Q. Q. Ji, G. J. Hou, X. W. Han, X. H. Bao, Y. Wang and D. H. Deng, Nat. Catal., 2021, 4, 242-250.

5. S. Zhou and H. C. Zeng, ACS Catal., 2022, 12, 9872-9886.

6. Y. Yuan, L. Qi, Z. Gao, T. Guo, D. Zhai, Y. He, J. Ma and Q. Guo, Molecules, 2023, 28, 5796.

7. Y. Zhou, F. Liu, S. Geng, M. Q. Yao, J. Ma and J. X. Cao, Mol Catal, 2023, 547, 113288.

8. S. Zhou, W. Ma, U. Anjum, M. Kosari, S. Xi, S. M. Kozlov and H. C. Zeng, Nat. Commun., 2023, 14, 5872.